Figure S1: Proximodistal heterogeneity of CA2/CA3 pyramidal neuron dendritic morphology

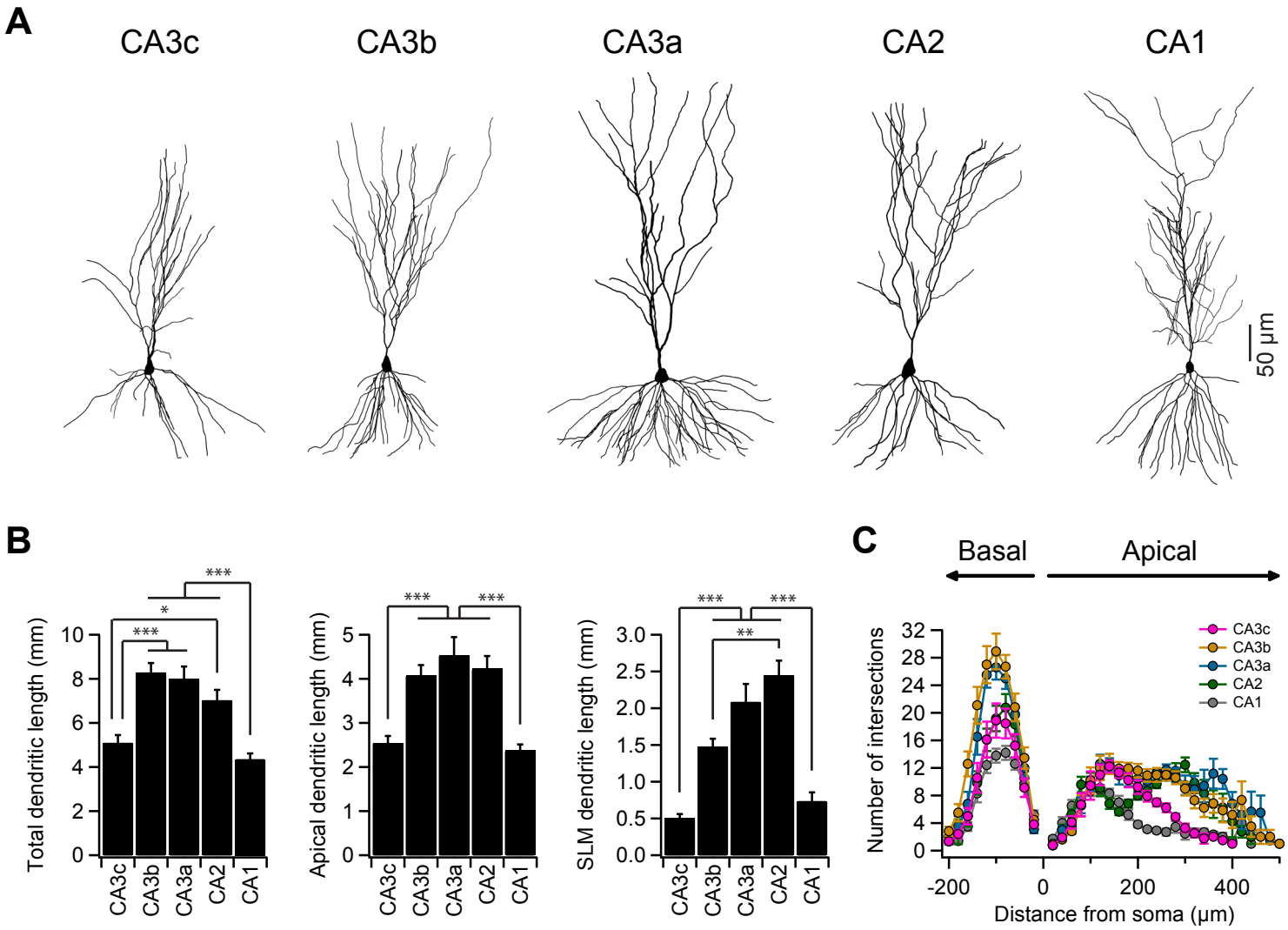

Figure S1, related to Figure 1. Proximodistal heterogeneity of CA2/CA3 pyramidal neuron dendritic morphology
(A) Representative morphology from biocytin-based reconstructions of hippocampal pyramidal neurons.
(B) Quantification of length (in mm) of total dendrites (left), apical dendrites (middle), and distal dendrites in SLM (right). Error bars show SE. ***p < 0.001, **p < 0.01, *p < 0.05. n = 9-12 neurons per group.
(C) Sholl analysis of dendritic branching patterns of CA2/CA3 pyramidal neurons across the proximodistal axis. n = 9-12 neurons per group.

Figure S2: A proximodistal gradient of intrinsic membrane excitability

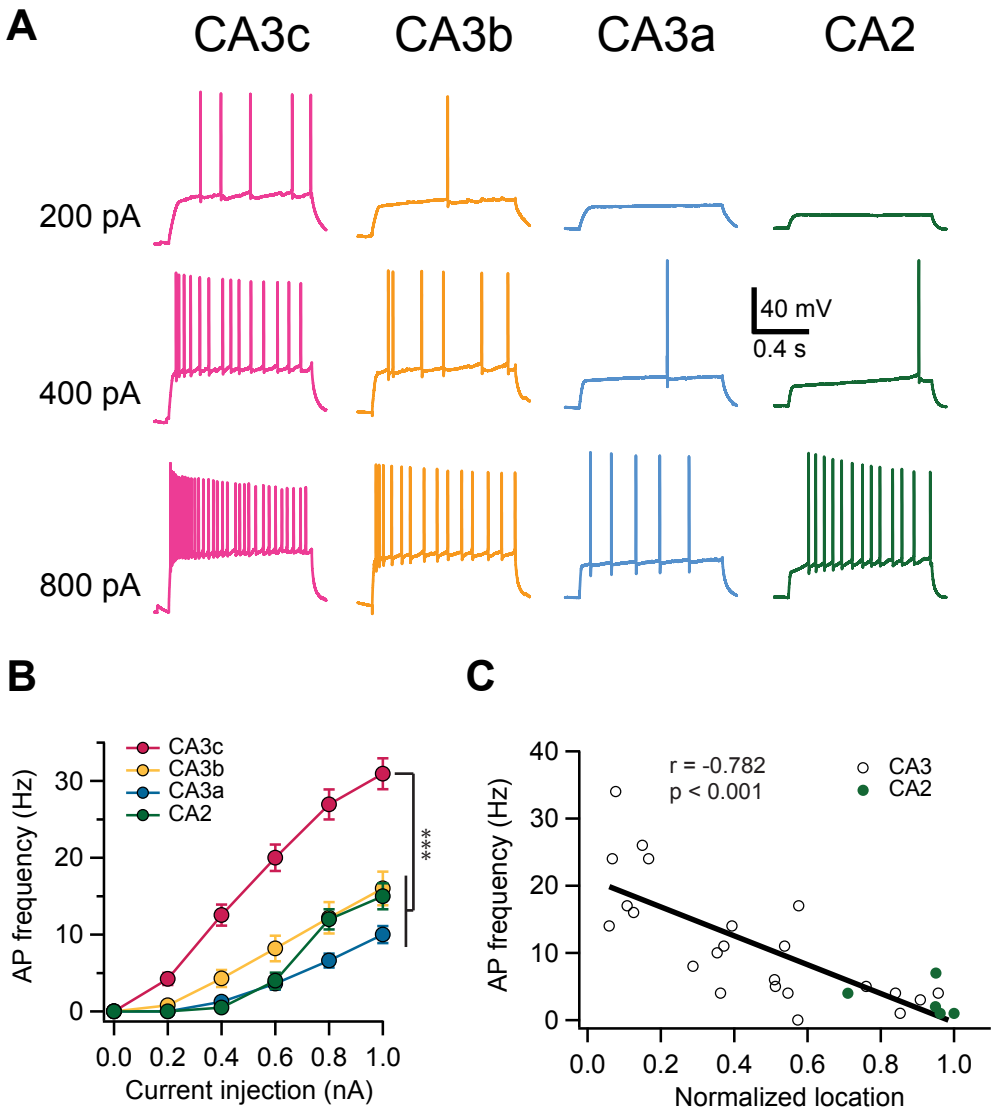

Figure S2, related to Figure 1. A proximodistal gradient of intrinsic membrane excitability
(A) Sample traces of firing patterns in response to constant current injection at the normal resting potential of each neuron.
(B) Relationship between mean firing frequency versus current injection from the resting potential. Error bars show SE. ***p < 0.001, n = 6-17 neurons per group.
(C) AP frequency in response to a 1 s, 600 pA current injection from the resting potential as function of normalized cell location along the proximodistal axis.

Figure S3: Active properties across the proximodistal axis.

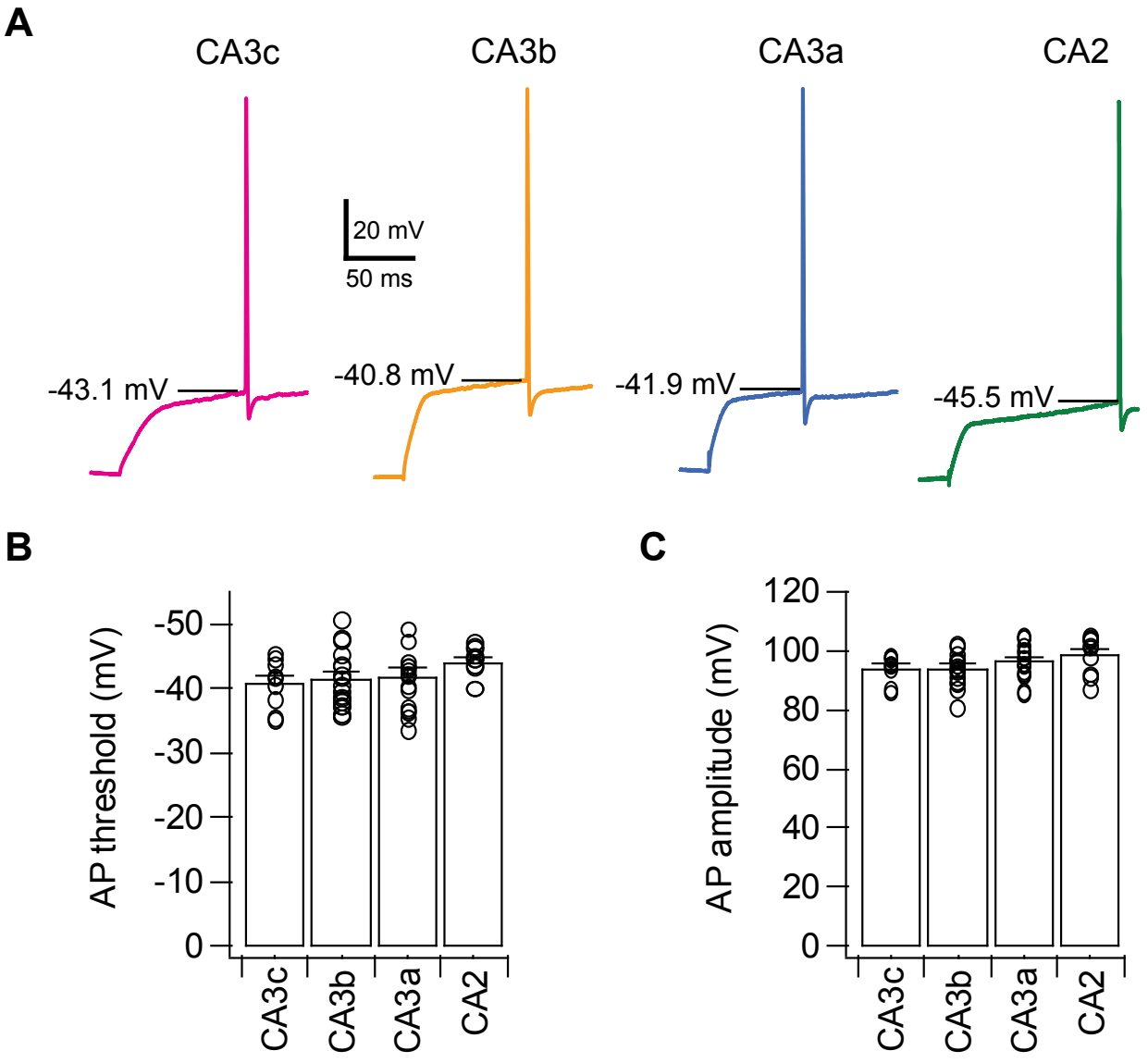

Figure S3, related to Figure 1. Active properties across the proximodistal axis.
(A) Sample traces of action potential threshold measurements.
(B) Mean voltage threshold of action potentials in CA2 and CA3 pyramidal neurons. n = 9-16 neurons per group.
(C) Mean amplitude of action potentials in CA2 and CA3 pyramidal neurons. Error bars show SE. n = 9-16 neurons per group.

Figure S4: Input resistance determines intrinsic excitability

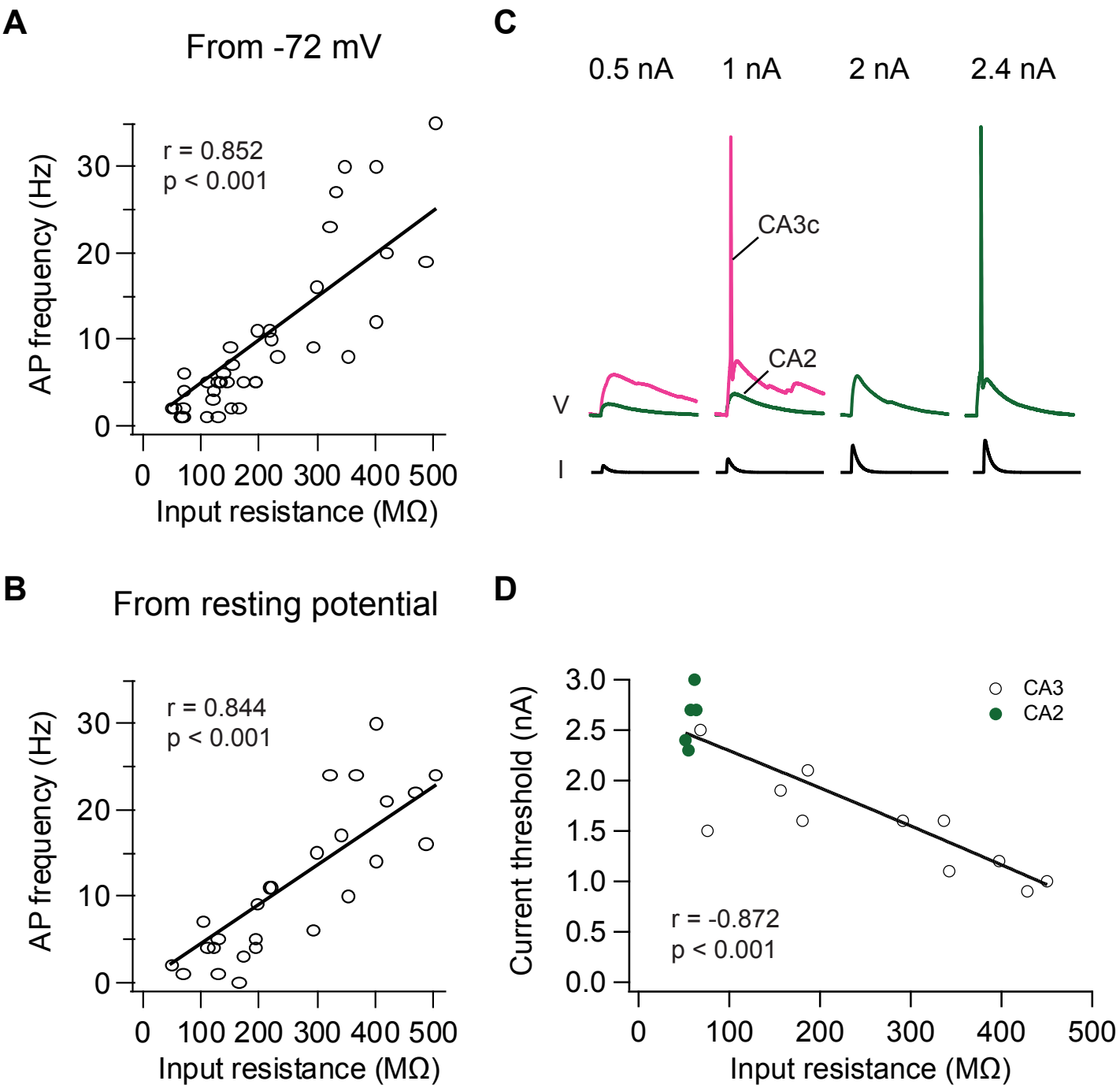

Figure S4, related to Figure 1. Input resistance determines intrinsic excitability
(A and B) AP frequency in response to a 1 s, 400 pA current injection plotted against input resistance, using an initial membrane potential of -72 mV (A) or the normal resting potential (B).
(C) Sample traces of membrane voltage responses to EPSC-like current injection.
(D) EPSC-like action potential current threshold plotted against input resistance.

Figure S5: Characterizing synaptic properties of the CA3 recurrent network

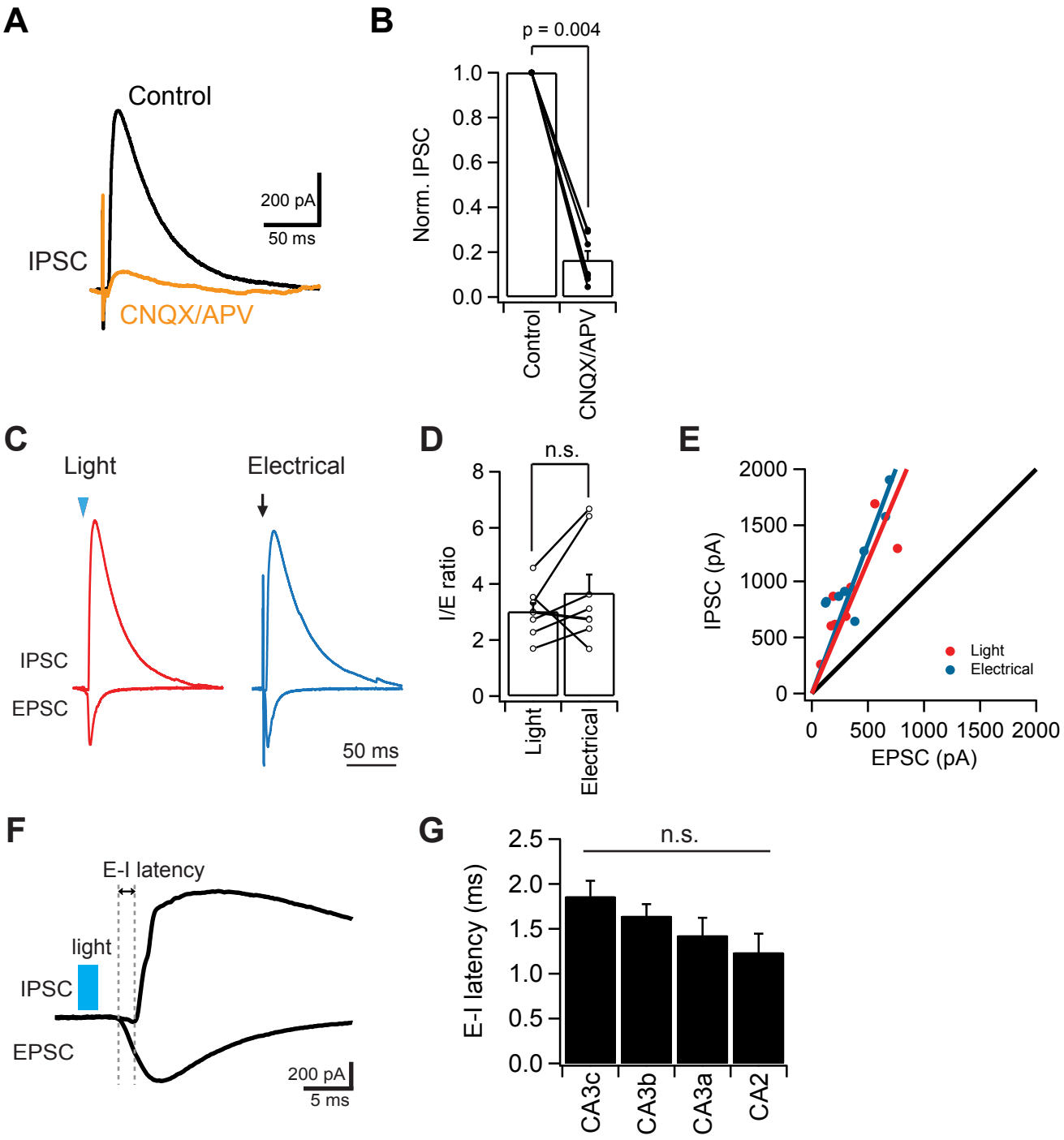

Figure S5, related to Figures 6,7. Characterizing synaptic properties of the CA3 recurrent network
(A) Sample traces showing blockade of glutamatergic synaptic transmission with D-APV (50 μM) and CNQX (20 μM) largely abolished the inhibition evoked by electrical stimulation of recurrent collaterals.
(B) Quantification of IPSC in the absence or presence of CNQX plus D-APV. Error bars show SE. n = 7 neurons.
(C) Sample traces showing the IPSC and EPSC evoked by either light or electrical stimulation of recurrent collaterals from the same CA3b pyramidal neuron. In this experiment, a small volume of AAV5-DIO-ChR2 was injected into the CA3 area in Grik4-Cre mice to express ChR2 specifically in CA3 pyramidal neurons.
(D) Quantification of the I/E ratio in response to light stimulation versus electrical stimulation. Error bars show SE. n.s., not significant. n = 8 neurons.
(E) IPSC is plotted against EPSC. Note the slope during light stimulation is comparable to that during electrical stimulation.
(F) Sample traces of an EPSC-IPSC sequence in response to a 2-ms light pulse recorded from a ChR2-negative CA3b pyramidal neuron. AAV-ChR2 virus was injected into the CA3 area 9 days before the recording.
(G) Quantification of the latency difference of the light-evoked EPSCs and IPSCs. n.s., not significant. ANOVA, p = 0.123. n = 6-9 neurons per group.